HIGH TEMPERATURE LOW CYCLE FATIGUE OF INCONEL MA 6000

J. Bressers
Materials Division
Joint Research Centre
P.O. Box 2
NL - 1755 ZG Petten

E. Arzt
Max-Planck-Institut für
Metallforschung
Seestrasse 92
D - 7000 Stuttgart 1

With data contributions from the following COST 501 projects: D48 (D. Froschhammer, H. Wilhelm), I9 (M. Marchionni), SF1 (V. Kuokkala, A. Hynnä), UK12 (I. Elliott, C. White)

ABSTRACT. Inconel MA 6000 is an oxide dispersion and γ'strengthened nickel base alloy and a candidate material for demanding high-temperature applications in corrosive environments. Its fatigue behaviour, which is not well documented, is explored in a collaborative action within the ODS group of COST 501. Cyclic deformation curves, cyclic stress-strain curves and cyclic life data are reported as a function of the applied strain-rate for the temperature range 760°C-1050°C. At 850°C the high strain fatigue results are correlated with high cycle fatigue data and compared to the performance of IN738LC. Microstructural analysis, in combination with the fatigue data, shows a transition to homogeneous deformation at approximately 800°C and a change from transgranular to mixed trans/intergranular failure at around 1000°C, which is thought to be triggered by environmental attack. The initiation of cracks appears to take up a considerable fraction of the cyclic life.

1. INTRODUCTION

Inconel MA 6000 is a candidate material for demanding high-temperature applications in corrosive environments (1). It combines the benefits of solid solution strengthening, strengthening by γ' for intermediate temperature strength and by Y_2O_3 particles for extreme elevated temperature strength. Its good oxidation resistance stems from an excellent oxide scale adherence which is promoted by the Y_2O_3 dispersion (2).

The outstanding performance of MA 6000 with regard to stress-rupture at high-temperature is well established (3,4). In order to avoid premature failure at grain boundaries, a highly elongated grain shape is essential (5). Only singular observations have been reported

about the behaviour of MA 6000 under fatigue loading, with much more emphasis on HCF than on LCF. An early study by WEBER and BOMFORD (6,7) indicated that the HCF resistance of a (low γ' volume fraction) ODS superalloy was higher, at room and elevated temperatures, than in the conventional counterpart of similar composition. It was observed that the transition from transgranular to mixed inter-transgranular fracture occurred at a temperature about 150°C higher than in conventional superalloys, which was attributed to both the elongated grain shape and the restrictive effects of the oxide dispersion on grain boundary sliding.
KIM and MERRICK (8) found simular results for MA 6000 E, an experimental variant of today's MA 6000. They detected an unusually high endurance ratio of 0.52. Also in low cycle fatigue at room temperature and 760°C the superiority of the ODS alloy over a cast superalloy (MAR-M200) was noted and, in contrast to conventional superalloys, dislocations were found to be homogeneously distributed.

The effect of specimen orientation with regard to the grain elongation on HCF of MA 6000 has been studied by HOFFELNER and SINGER (9). The results indicate that specimens loaded in a direction transverse to the grain elongation exhibited reduced HCF strength, but were still within the scatterband for IN738LC and IN939. Crack growth rates in air, however, were measured to be lower in this direction than in the longitudinal direction.

This short review of the literature on fatigue of MA 6000 and related alloys emphasizes the need for a more systematic study of the fatigue behaviour, in particular of LCF, of MA 6000. Within the ODS group of COST 501 this objective has been pursued, with the aim of, first, establishing a broader data base and, second, carrying a step further the explanations for the observed behaviour on the basis of microstructural investigations. Some of the results obtained will be reported in this paper.

2. MATERIALS AND METHODS

2.1 Material

The Inconel MA 6000 material was supplied in the form of a flat, zone annealed bar by one of the collaborating COST projects (UK12). The heat treatment - 1 hr/1232°C/AC, 2hrs/954°C/AC, 24 hrs/845°C/AC - was designed to give optimum properties at very high temperatures. The nominal composition of this particular cast, in weight percent, is given in Table I.
The oxide phase contains Y and Al, which is oxidized and incorporated in the Y_2O_3 phase during processing. The volume fractions of the γ' and Y_2O_3 phases, which were determined through quantitative extraction and X-ray analysis, are 48.8 vol% and 1.7 vol% (0.96 wt%) respectively. The latter figure is based on the assumption that the composition of the oxide phase is $(YAl)_2O_3$.
The material contains occasional processing defects such as

TABLE I - Chemical composition (wt.%)

Cr	Ti	Al	Mo	W	Ta	Ni	Y_2O_3	Fe	Zr
15.03	2.38	4.38	2.02	3.97	1.97	bal	1.13	0.72	0.16

Cu	Mn	C	Si	S	N	O	B
<.01	0.01	0.050	0.06	0.002	0.15	0.42	88ppm

unrecrystallized regions, milling defects and particle stringers. The high-temperature zone annealing of the mechanically processed MA 6000 gives rise to a highly elongated grain structure in the hot working direction, with a grain aspect ratio of the order of ten. The elongated grain structure has a pronounced <110> texture.
The results reported in the present paper are for longitudinal samples, i.e. the loading direction coincides with the long axis of the grains.

2.2 Testing Conditions

The fatigue behaviour of MA 6000 is being explored by several collaborating COST 501 projects. Whilst each project aims to achieve its individual objective, it was decided to commonly generate a baseline set of LCF data which could be used for comparison against individual project data. The work-sharing matrix encompasses tests at various temperatures in air. The applied wave shape is triangular and symmetrical ($R_\varepsilon = -1$). The tests are performed in strain control between total, axial strain limits, unless otherwise stated. The strain rates range from $\dot{\varepsilon}_t = 1.10^{-2}\ s^{-1}$ to $\dot{\varepsilon}_t = 2.10^{-5}\ s^{-1}$.
The specimen design, the details of the specimens machining (with the exception of a prescribed surface finish of $R_a = 0.2\ \mu m$ or better) and the method of heating of the specimen to the test temperature, were left at the discretion of each project. In view of the limited ductility of MA 6000, the participants were asked to limit the bending strain on the gauge length surface to ± 5% of the minimum axial strain amplitude applied in the testing programme.

2.3 Microstructural Analysis

The microstructures of as-received and of fatigued specimens were investigated with the usual methods. Light microscopy and SEM to detect and analyse damage processes were employed on polished sections which had been carefully prepared in order to avoid metallographic artefacts. 3-D fractography revealed information about initiating defects and the morphology of the fracture path. In addition, the dislocation configurations that had developed during LCF were studied by TEM.

3. RESULTS

3.1 Low Cycle Fatigue Data

A selection of cyclic deformation curves is shown in Figure 1. A considerable inter-specimen variability of the cyclic stress levels on these curves is sometimes observed, as illustrated by the set of curves marked A in the figure. The fact that these curves were generated in different laboratories does not necessarily imply an interlaboratory variability, since similar differences are sometimes observed among specimens tested in one laboratory.
The number of cycles to failure, though, shows good agreement (see below). The failure of the specimens is preceded by a very sudden drop in the stress range, allowing the straightforward application of a stress drop based fracture criterion.
Broadly speaking, two types of cyclic deformation curves are observed. Specimens deformed at high strain amplitudes and high strain rates exhibit cyclic softening early in their lives, followed by cyclic saturation. Small strain amplitudes, low strain rates and high temperatures promote cyclic saturation from the first cycle onwards, although slight cyclic hardening is occasionally noted during the first stages in the life. Figure 1 also illustrates the severe drop in cyclic stress which results from an increase in the testing temperature and from a decrease in the strain rate.

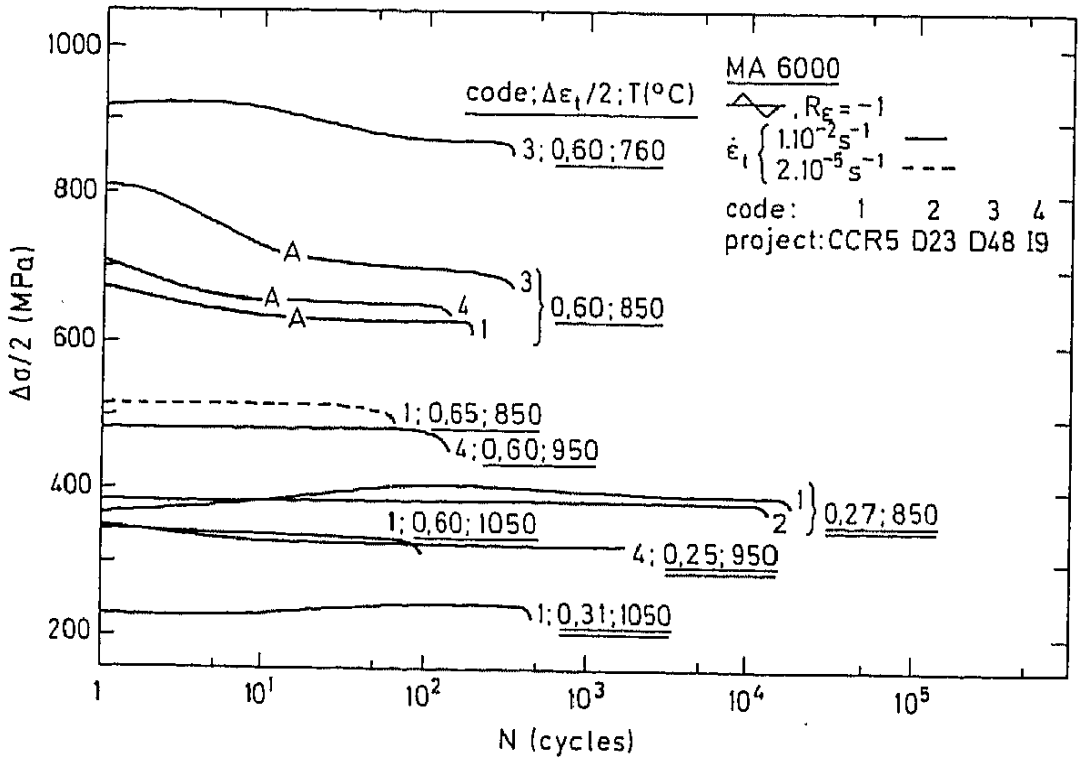

Fig.1 : Cyclic deformation curves of MA 6000.

The cyclic stress strain curves plotted in Figure 2 are based on the relationship between the applied total strain amplitude and the cyclic stress response at half life. The numerical data are also listed in Table II, grouped according to the COST 501 projects which generated the data set. The comparison of the MA 6000 data at T = 850°C, $\dot{\varepsilon}_t = 1.10^{-2}\,s^{-1}$ with IN738LC data stemming from earlier COST projects (10,11) shows the slightly superior cyclic strength of IN738LC at the higher strain amplitudes.

The "quality" of the data sets generated in each laboratory was checked by means of round robin tests at T = 850°C, $\dot{\varepsilon}_t = 1.10^{-2}\,s^{-1}$. The corresponding cyclic lives are plotted in Figure 3 as a function of the total and of the plastic strain amplitudes. The plastic strain amplitudes are calculated on the basis of the cyclic stresses at half-life, using either the static E-moduli measured during the test or the value of the E-modulus reported by project CH6. The $\Delta\sigma$ levels of the tests performed by project UK12 were converted to strain amplitudes by means of the corresponding cyclic stress-strain curve in fig. 2 (triangular symbols). Some recent high-cycle fatigue data are included as well (9). The scatter in the total strain amplitude-cyclic life data is quite small if one considers the interlaboratory differences in testing techniques and the anticipated variability in the materials fatigue properties as the result of the large, columnar grain size. In terms of its dependence on the plastic strain amplitude, $\Delta\varepsilon_p$, the scatter in the cyclic lives, in particular at the smaller strain amplitudes, is large. The calculated $\Delta\varepsilon_p$ values are indeed subject to a large uncertainty since even a limited degree of

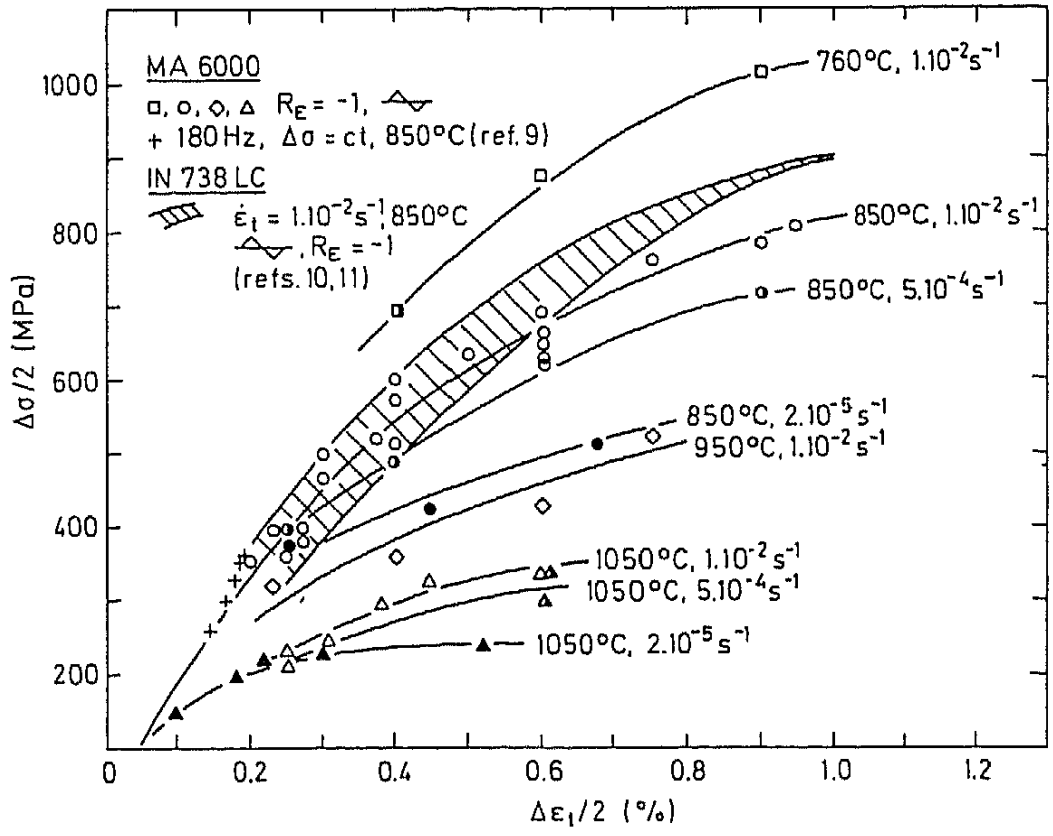

Fig. 2 : Cyclic stress-strain curves of MA 6000: comparison with IN738LC

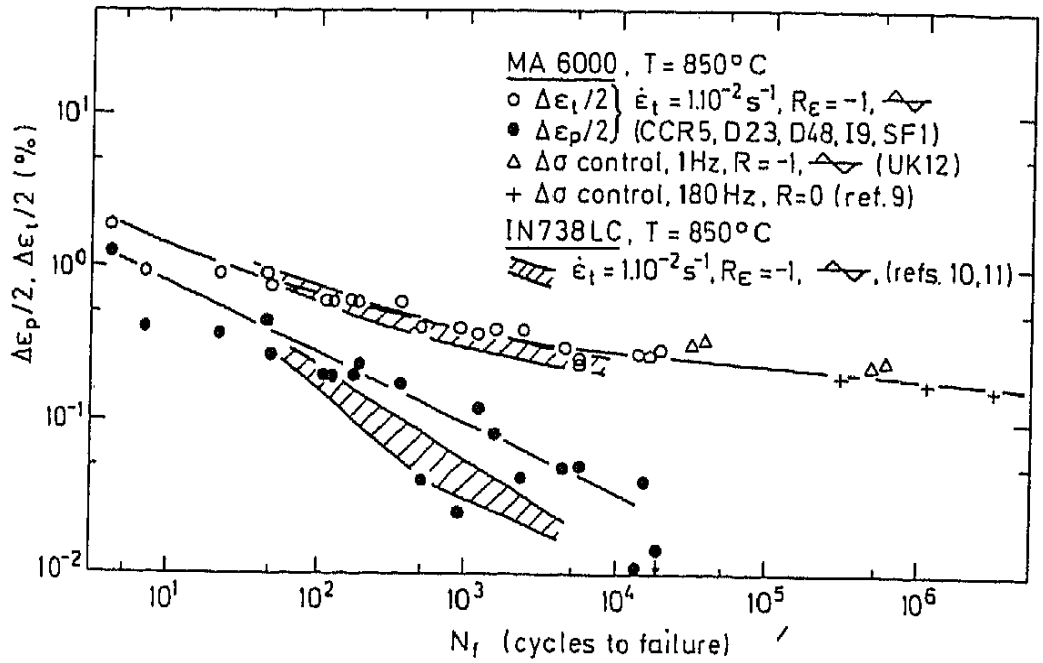

Fig. 3 : Cyclic lives of MA 6000 at 850°C, $\dot{\varepsilon}_t = 1.10^{-2}s^{-1}$ as a function of the total and of the plastic strain amplitude; comparison with IN738LC.

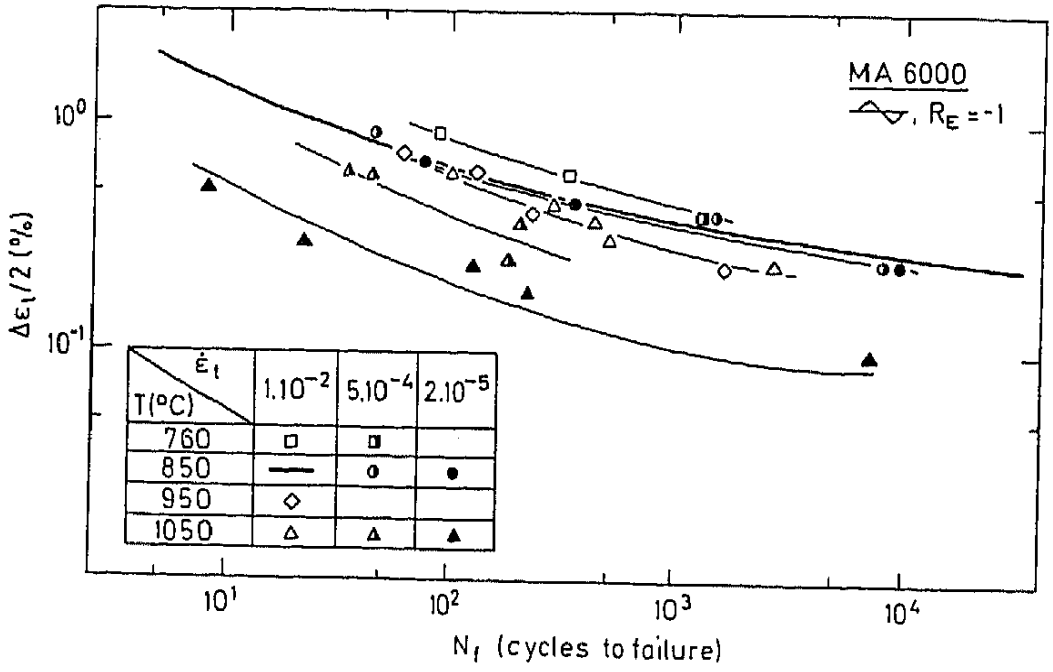

Fig. 4 : Strain-rate and temperature dependence of the cyclic life of MA 6000.

variability in the cyclic stress results in large changes in $\Delta\varepsilon_p$ when the elastic strain amplitude approaches the total strain amplitude. The cyclic lives of MA 6000 and of IN738LC are comparable when expressed in terms of the total strain amplitude. The data in fig. 3 suggest that MA 6000 is more resistant than IN738LC when subjected to similar plastic strain ranges.

The dependence of the cyclic lives on the testing temperature and

on the strain rate is plotted in fig. 4 as a function of the total strain amplitude. The heavy line is the best fit through the data points at T = 850°C, $\dot{\varepsilon}_t = 1.10^{-2} s^{-1}$. Higher temperatures and/or lower strain rates enhance the effect of time dependent damaging processes on the fatigue life. The indifference of the cyclic lives with respect to the reduction in strain rate at 850°C suggests that the effect of time dependent damage up to that temperature is small. The further increase in the testing temperature to 1050°C is marked by a strong influence of the strain rate on the life.

3.2. Fracture mode and microstructural damage

Unlike crept specimens, the fatigued samples do not show any extensive internal damage apart from localized damage in unrecrystallized regions or at milling defects. These are however non-propagating and do not influence the fracture behaviour. This is illustrated by the fractograph of a specimen tested at a temperature of 850°C and a strain rate of $\dot{\varepsilon}_t = 1.10^{-2} s^{-1}$ in fig. 5. The crack which led to failure of the sample initiated at the surface on the right hand side of the fractograph, and propagated in the direction indicated by the arrow. The extended defect area at the upper left did not contribute to crack nucleation. Fig. 5 also shows one of the larger defects in the upper left area. The defects are often hollow particles surrounded by shells which are highly enriched in Ni and S.
At 1050°C the fracture surfaces look totally different. The increase in test temperature is marked by a transition from a purely transgranular

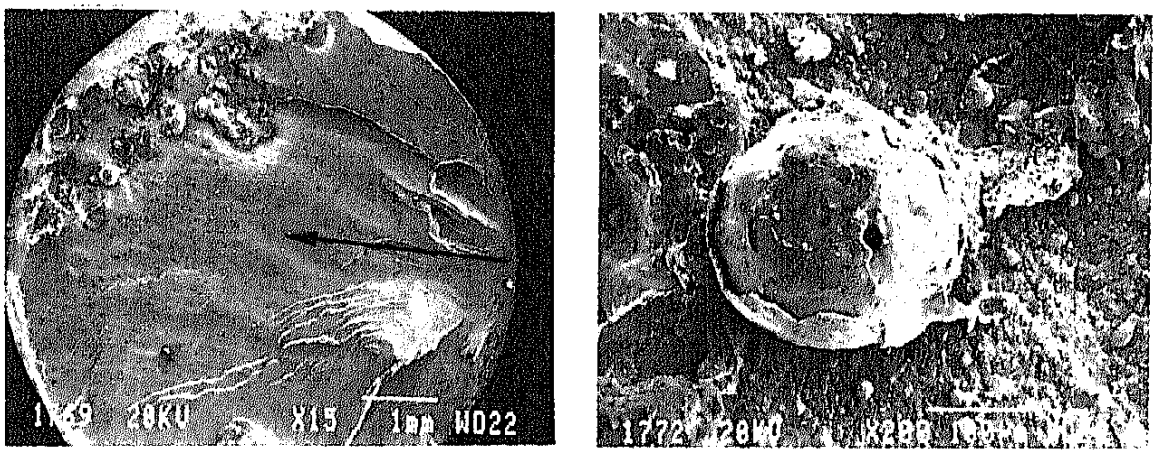

Fig. 5 :Fracture surface of a sample fatigued at T = 850°C, $\dot{\varepsilon}_t = 1.10^{-2} s^{-1}$, $\Delta\varepsilon_t/2 = 0.27$ %, showing crack propagation direction (arrow), milling defect area (left) and defect detail (right).

to a mixed trans/intergranular crack propagation. A typical fracture surface appearance is shown in fig. 6 for a sample fatigued at T = 1050°C, $\dot{\varepsilon}_t = 5.10^{-4} s^{-1}$. Grain boundary cracking in the longitudinal direction results in the pull-out of individual grains following transgranular crack growth across the grain sections.
Cracks invariably nucleate at the specimen surface in a transgranular mode (fig. 7). Occasionally intergranular crack initiation may be

observed where grain boundaries intersect the surface, in particular under the high test temperature/low strain rate conditions which hold for the sample shown in fig. 7. The parallelism of the surface cracks in the single surface grain of fig. 7 suggests crystallographic stage I cracking in the early phase of the crack growth process. After the crack has advanced over some distance, further crack growth proceeds through a stage II striation growth mechanism. Multiple transgranular crack initiation without any sign of intergranular cracking was observed on the surface of the sample in fig. 8, fatigued at T = 1050°C and $\dot{\varepsilon}_t = 1.10^{-2}\,s^{-1}$.

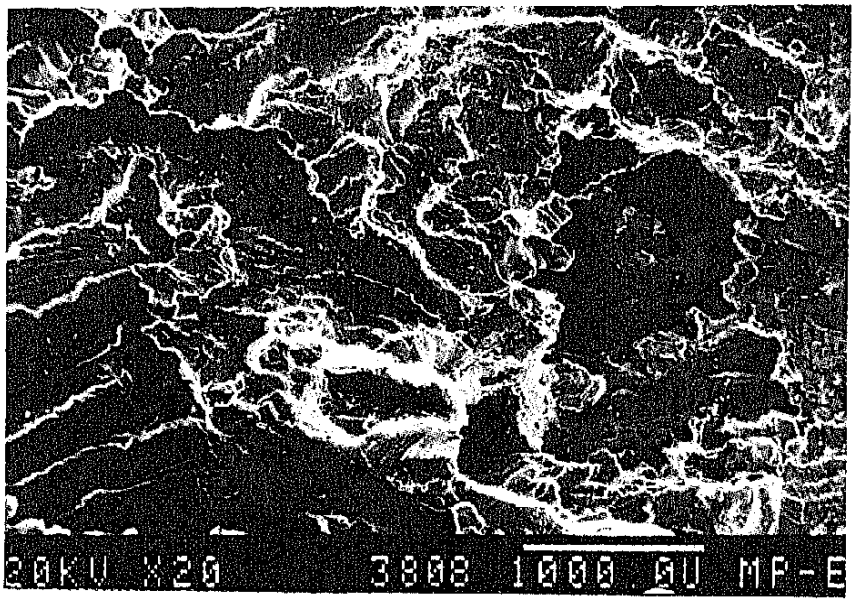

Fig.6 : Mixed trans/intergranular crack propagation in a specimen tested at T = 1050°C, $\dot{\varepsilon}_t = 5.10^{-4}\,s^{-1}$, $\Delta\varepsilon_t/2 = 0.40$ %. Note striations and grain pull-out (from ref. 12).

Fig.7 :Surface cracks in a specimen tested at T = 1050°C, $\dot{\varepsilon}_t = 5.10^{-4}\,s^{-1}$, $\Delta\varepsilon_t/2 = 0.6$ % (from ref.12).

The cracks are covered with nickel-rich oxide crystallites whose morphology and chemical composition are unlike the oxide covering the

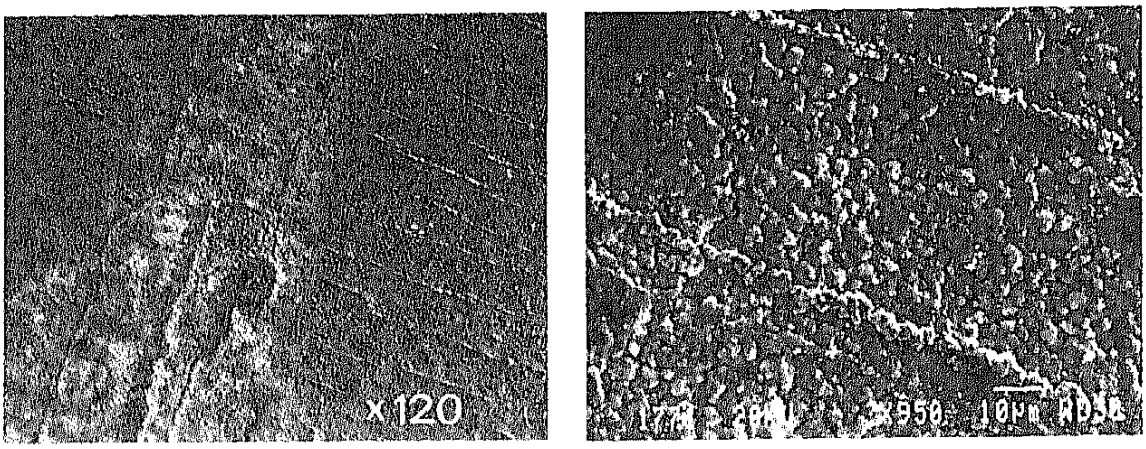

Fig. 8 :Surface crack initiation in a direction perpendicular to the loading axis (left); oxide morphology on top of the cracks (right). Specimen cycled at T = 1050°C, $\dot{\varepsilon}_t = 1.10^{-2}\ s^{-1}$, $\Delta\varepsilon_t/2 = 0.25$ %.

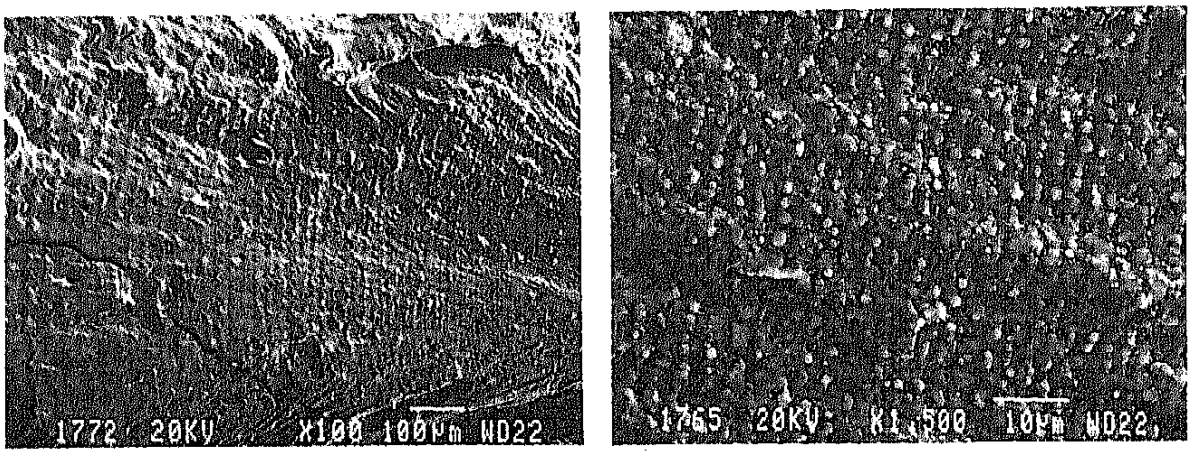

Fig. 9 :Striations on a specimen fatigued at T = 850°C, $\dot{\varepsilon}_t = 2.10^{-5}$ and $\Delta\varepsilon_t/2 = 0.45$ % (left). Note globular oxidation product (right).

non-damaged surface area.Fig. 9 gives examples of the striations observed on the fracture surface of a sample fatigued at T = 850°C, $\dot{\varepsilon}_t = 2.10^{-5}\ s^{-1}$ and $\Delta\varepsilon_t/2 = 0.45$ %. The globular particles (right) are thought to be oxidized γ' precipitates.

Typical dislocation configurations in samples deformed at T = 850°C, $\dot{\varepsilon}_t = 1.10^{-2}\ s^{-1}$ are shown in fig. 10. Dislocation networks, formed by climb, surround the γ' precipitates, in particular at the high strain amplitudes. The dislocations are anchored at yttria particles. Occurrence of networks distinguishes the dislocation structure from configurations after creep exposure, where only single dislocations are seen to interact with the dispersoids.

4. DISCUSSION

The scatter of the round robin data at T = 850°C, $\dot{\varepsilon}_t = 1.10^{-2} s^{-1}$ is surprisingly low, both in terms of the levels of the cyclic stress response and of the cyclic lives when related to $\Delta\varepsilon_t/2$. This lends confidence to the data sets which were generated by the participating projects at the other test temperatures and strain rates.

Nickel-based alloys which are strengthened by γ'precipitates deform by a mechanism in which the γ'particles are either sheared or bypassed by the dislocations. The lack of any substantial hardening, and the saturation of the cyclic stress observed in most of the experiments, point to a dislocation bypassing mechanism. The dislocation networks which surround the γ'particles and the absence of any stacking fault contrast in the γ'phase at temperatures of 850°C and above, confirm this. At 760°C and at strain rates of the order of $\dot{\varepsilon}_t = 1.10^{-4} s^{-1}$, cutting of the γ' in MA 6000 was recently reported (14). Hence, the mode of deformation changes from shear to dislocation bypassing, with a concurrent homogenization, at around 800°C under the strain rate conditions here applied.

The TEM micrographs in fig. 10 reveal a striking detail on close inspection : obviously an attractive interaction between dislocation and yttria dispersoids exists, leading to "departure" side pinning of the dislocation. This is also a characteristic feature in crept MA 6000 where it has been studied in detail (13). The implications of this strengthening mechanism for LCF behaviour are the subject of current work in COST 501.

At elevated temperatures, time dependent processes increasingly contribute to the deformation and damage development in fatigue. The reduction of the cyclic life with decreasing strain rate forms evidence

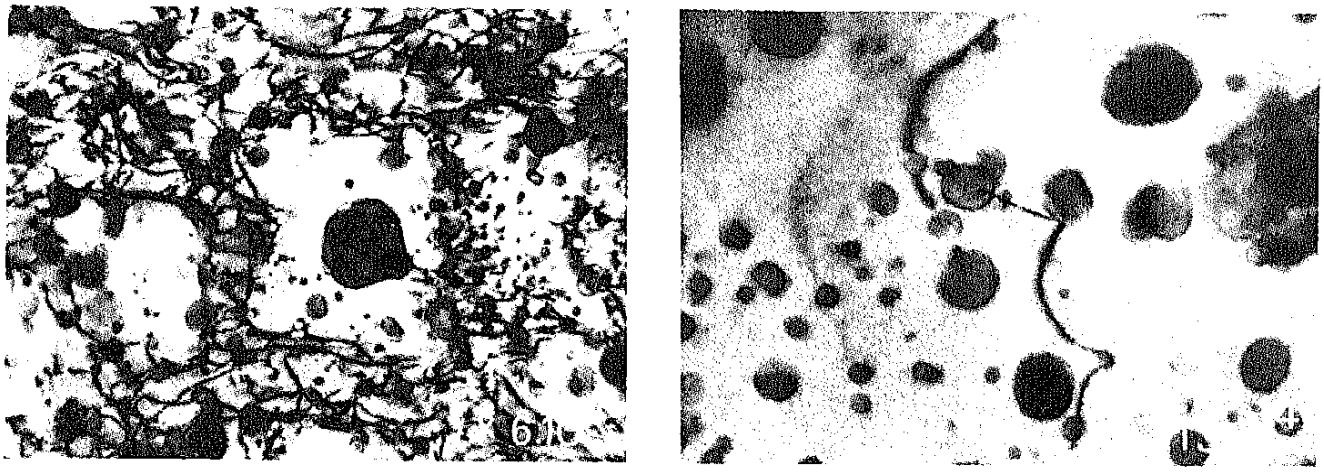

Fig. 10 :TEM micrographs showing dislocation network developed during cycling at T = 850°C, $\dot{\varepsilon}_t = 1.10^{-2} s^{-1}$, $\Delta\varepsilon_t/2 = 0.45$ % (left). Note "departure" side pinning of a dislocation at the yttria dispersoids.

for the interaction of the fatigue process with creep, oxidation or microstructural degradation processes. Fig. 4 shows that substantial strain rate effects are exhibited only for temperatures in excess of approximately 900°C. In conventional, γ'strengthened superalloys, similar effects occur at appreciably lower temperatures because of the activation of grain-boundary fracture paths. The good oxidation resistance and the nearly complete absence of transverse grain boundaries in longitudinal samples of MA 6000 are beneficial in that respect.
First observations show that internal, cavitation type damage on grain boundaries does not develop, notwithstanding the failure of samples along mixed inter/transgranular fracture paths at 1050°C. It therefore appears quite likely that the reduction in life largely results from some form of oxygen attack. It is anticipated that the penetration of oxygen along surface cracks and grain boundaries, and subsequent oxide formation (visible in fig. 7 as a white layer running along the specimen surface and the surface cracks) exerts a strong influence on the crack initiation process in particular. Such environmental effects will be the subject of further investigations.

If one defines the number of cycles for crack initiation as the fraction of the cyclic life used to initiate and grow a microcrack to an easily detectable size of some ten micrometers, then crack initiation usually covers a small fraction of the low cycle fatigue life. In MA 6000 however, the initiation phase takes up a significant portion of the fatigue life. First estimates of this initiation life fraction are based on a quantitative analysis of fatigue striations on the fracture surface of a specimen cycled at T = 950°C, $\dot{\varepsilon}_t = 2.10^{-5}\,s^{-1}$, $\Delta\varepsilon_t/2 = 0.25$ % and on the measurement of surface crack lengths on replicas made at increasing cycle numbers on a sample fatigued at T = 1050°C, $\dot{\varepsilon}_t = 1.10^{-2}\,s^{-1}$, $\Delta\varepsilon_t/2 = 0.45$ %. In both instances, $N = N_f/3$ to $N_f/2$ cycles are required to initiate cracks with a depth of approximately 50 μm. Subsequent crack growth occurs at very high rates, as can also be anticipated on the basis of the sudden drop in the cyclic deformation curves near to N_f (fig. 1).

5. CONCLUSIONS

1. A data base for the high-temperature LCF behaviour of MA 6000 has been established. Its cyclic life is comparable with that of IN738LC when expressed in terms of the total strain aplitude, and better when subjected to similar plastic strain ranges.

2. Fatigued samples do not show extensive internal damage. Fracture is transgranular at 850°C and becomes mixed inter/transgranular at 1050°C, possibly because of environmental attack.

3. At the strain rates studied, the deformation mode changes from dislocation shearing of γ' precipitates to bypassing, with a concurrent homogenization at about 800°C.

4. Crack initiation takes up a significant portion of the fatigue life and is aided by oxidation to a higher extent than would be expected on the basis of the good oxidation resistance of the alloy.

6. ACKNOWLEDGEMENT

The authors are grateful to the COST 501 project leaders for their permission to use their "baseline test matrix" LCF data. They also acknowledge the skilled assistance of Messrs. E. Fenske (J.R.C.) for the mechanical testing of P. Tambuyser, P. Helbach (J.R.C.) and G. Hamburg (E.C.N.) for their help with the microstructural analysis, and the contributions of H. Zeizinger and D. Elzey.

Table II - COST 501 Low Cycle Fatigue Data

Project	Strain rate (s^{-1})	Temp. (°C)	Strain-range (%)			Cyclic stress Range (MPa)			N_f (cycles)
			$\Delta\varepsilon_t$	$\Delta\varepsilon_e$	$\Delta\varepsilon_p$	σ_{max}	σ_{min}	$\Delta\sigma$	
CCR5	1.10^{-2}	850	0.54	0.46	0.08	395	405	800	16100
			0.59	0.49	0.10	460	478	938	4944
			0.75	0.63	0.12	528	525	1053	1365
			1.23	0.75	0.48	599	637	1236	194
			1.89	0.95	0.94	761	851	1612	49
	2.10^{-5}	850	0.50	0.44	0.06	380	380	760	9400
			0.90	0.57	0.33	456	481	837	352
			1.36	0.62	0.74	499	530	1029	73
	1.10^{-2}	1050	0.50	0.33	0.17	230	243	473	2700
			0.62	0.31	0.31	242	244	486	520
			0.76	0.38	0.38	292	298	590	432
			0.89	0.44	0.45	325	333	658	288
			1.20	0.43	0.77	327	338	665	100
D23	1.10^{-2}	850	0.55	0.53	0.02	429	338	767	13082
			0.79	0.74	0.05	525	504	1029	904
			1.81	1.08	0.73	740	806	1546	22
	5.10^{-4}	1050	0.50	0.32	0.18	196	207	403	173
			0.79	0.27	0.52	188	200	388	199
			1.20	0.42	0.78	279	307	586	34
			1.21	0.47	0.74	327	341	668	44

Project	Strain rate (s^{-1})	Temp. (°C)	Strain-range (%)			Cyclic stress range (MPa)			N_f (cycles)
			$\Delta\varepsilon_t$	$\Delta\varepsilon_e$	$\Delta\varepsilon_p$	σ_{max}	σ_{min}	$\Delta\sigma$	
D48	1.10^{-2}	760	1.20	0.96	0.24	839	911	1750	330
			1.80	1.20	0.60	989	1075	2064	86
	5.10^{-4}	760	0.80	0.74	0.06	659	725	1384	1331
	1.10^{-2}	850	0.60	0.59	0.01	478	532	1010	20490
			0.80	0.72	0.08	595	615	1210	2287
			1.20	0.88	0.32	669	721	1390	356
	5.10^{-4}	850	0.50	0.50	0	400	404	804	7996
			0.80	0.64	0.16	485	499	984	1492
			1.80	0.98	0.82	681	749	1430	45
I9	1.10^{-2}	850	0.47	0.47	0	395	400	795	5105
			0.80	0.72	0.08	573	593	1166	490
			1.21	0.80	0.41	595	648	1293	185
			1.21	0.83	0.38	624	673	1297	125
			1.21	0.84	0.37	633	695	1328	115
			1.50	0.98	0.52	724	807	1531	50
			1.81	1.00	0.81	743	822	1565	7
	1.10^{-2}	950	0.46	0.44	0.02	318	330	648	1600
			0.81	0.50	0.31	398	417	715	230
			1.21	0.67	0.54	456	498	854	135
			1.50	0.75	0.75	512	554	1066	60
SF1	1.10^{-3}	850	0.50	0.40	0.10	704			5123
			1.00	0.70	0.30	632			72
			3.60	1.02	2.58	830			4
	2.10^{-5}	1050	0.20	0.18	0.02	150			>6800
			0.36	0.22	0.14	195			210
			0.44	0.26	0.18	220			122
			0.60	0.26	0.34	228			22
			1.24	0.28	0.76	235			8
UK12	stress control $R_\sigma = -1$								
	1Hz	850	0.48			383	383	766	$6,14.10^5$
			0.49			395	395	790	$4,66.10^5$
			0.66			484	484	968	$4,11.10^4$
			0.68			492	492	984	$3,53.10^4$

Unless otherwise noted, cycling is triangular with $R_\varepsilon = -1$, in strain control between total strain limits. Environment : air.

7. REFERENCES

1. SINGER, R.F. and E. ARZT, 'Processing, Structure and Properties of ODS Superalloys', this volume.
2. WHITTLE, D.P. and J. STRINGER, 'Improvements in high temperature oxidation resistance by additions of reactive elements or oxide dispersions', Phil.Trans. R. Soc. Lond. A295 (1986), 309.
3. SINGER, R.F., R.C. BENN and S.K. KANG, 'Creep Rupture Properties of Inconel Alloy MA 6000', in Frontiers of High Temperature Materials II, Inco Alloy Products Company, 1983, p.336.
4. BENN, R.C. and S.K. KANG, 'Long-Term Mechanical Behaviour of Some ODS Alloys', in Superalloys 1984, M. Gell et al., eds., TMS-AIME, 1984, p.321.
5. ARZT, E. and R.F. SINGER, 'The Effect of Grain Shape on Stress Rupture of Inconel MA 6000', in Superalloys 1984, M. Gell et al., eds., TMS-AIME, 1984, p.367.
6. WEBER, J.H. and M.J. BOMFORD, 'High-Cycle Fatigue Properties of a Dispersion Strengthened Nickel-Base Superalloy', in Fatigue at Elevated Temperatures, ASTM STP 520, Carden et al., eds, Philadelphia, PA, 1972, p.427.
7. WEBER, J.H. and M.J. BOMFORD, 'Comparison of Fatigue Deformation and Fracture In a Dispersion-Strengthened and a Conventional Nickel-Base Superalloy", Metall. Trans. 7A (1973), p.435.
8. KIM, Y.G. and H.F. MERRICK, 'Fatigue Properties of MA 6000 E, a γ-Strengthened ODS Alloy", in Superalloys 1980, J.K. Tien et al., eds, ASM, Metals Park, OH, 1980, p.551.
9. HOFFELNER, W. and R.F. SINGER, 'High Cycle Fatigue Properties of the ODS Alloy MA 6000 at 850°C', Metall. Trans 16A, 1985, p.393.
10. THOMAS, G.B and R.K. VARMA, 'Assessment of LCF and creep-fatigue behaviour of Ni-Cr base supperalloys', Project UK-11, COST 50/II, final report, 1984.
11. HOFFELNER, W., M. NAZMY, and C. WÜTHRICH, 'Life Time Prediction of gas turbine components', Project CH-2, COST 50/III, final report, 1984.
12. ZEIZINGER, H., D. ELZEY and E. ARZT, to be published (1986).
13. ARZT, E. and J.H. SCHRÖDER, 'High temperature strength of ODS superalloys due to dispersoid-dislocation interaction', this volume.
14. HUIS IN 'T VELD, E.J., P.M. BRONSVELD, J.Th.M. DE HOSSON and J. BRESSERS, 'Dislocation microstructure in PM Astroloy and MA 6000 after HTLCF', Conference 'High Temperature Alloys : Their Exploitable Potential, Petten, Oct. 15-17, 1985.